Geophysical Research Letters

Supporting Information for

Statistical Downscaling of Seasonal Forecast of Sea Level Anomalies for US Coasts

Xiaoyu Long[1,2], Sang-Ik Shin[1,2] and Matthew Newman[1,2]

[1]CIRES, University of Colorado Boulder, Boulder, CO, USA
[2]NOAA Physical Sciences Laboratory, Boulder, CO, USA

Contents of this file

Text S1: Optimal Truncation

Since we built the linear regression in EOF space, we examined its sensitivity to the number of EOFs retained for each field in the regression, evaluating how EOF truncation impacted the downscaling operator's ability to reproduce the fine-scale GLORYS data from the coarse-grained GLORYS data. The downscaling was calculated using a 10-fold cross-validation, where 90% of the data was used to determine the operator, which was then used to downscale the remaining 10%; this process was cycled through ten times. As a metric of the goodness of fit for the resulting downscaled data, we computed the correlation between the downscaled fine-scale SSH anomalies and the original fine-scale SSH anomalies, evaluated along both time and spatial dimensions. Fig. S2a and d show this metric as a function of both predictor and predictand EOF truncation. For the West Coast, the best fit occurred with 34 /10 EOFs retained for the predictor/predictand. Additional EOFs eventually degrades the accuracy of the downscaling. For the East Coast, the best fit occurred for predictor/predictand truncation of 40/5 EOFs.

Text S2: SVD of the downscaling operator

What the downscaling operator (regression matrix) does is mapping the predictor space to the predictand space. SVD (singular vector decomposition) of the downscaling operator will help us better understand what modes in the predictor and predictand spaces contribute most to the downscaling.

The SVD of the downscaling operator is done as follows:

$$\mathbf{y} = \mathbf{B}\mathbf{x}$$
$$\mathbf{B} = \mathbf{U}\boldsymbol{\Sigma}\mathbf{V}^{\mathbf{T}}$$
$$\mathbf{y} = \mathbf{U}\boldsymbol{\Sigma}\mathbf{V}^{\mathbf{T}}\mathbf{x}$$

The column vectors in U constitute an orthonormal basis that spans the space of y, and the column vectors in V span the space of x. $\boldsymbol{\Sigma}$ is a diagonal matrix and its diagonal values are the singular values of the SVD of **B**. In principle, the downscaling operator projects the predictor x onto each of the singular vector in V, then weights the projection by corresponding singular value, and finally multiplies by the singular vector in U. The relative magnitude of the singular vectors in V and the singular vector in U weighted by corresponding singular values indicates the pattern that has been amplified or damped in the downscaling process.

The dominant three singular vector pairs for each downscaling operator are shown in Fig. S4-5. Note that the relative magnitude difference between the left and right singular vectors indicates whether this specific structure was amplified or damped by the

downscaling operator. For the west coast, the first singular vector pair (top row in Fig. S5) shows a pattern with the same sign all along the coast that is amplified by the downscaling, and likewise dominates the downscaling skill improvement (see Fig. S6). The second singular vector pairs is a dipole-like pattern also confined to the coast, amplified primarily in the Southwest coast. These patterns presumably represent effects of different phases of coastal Kelvin waves. The third singular vector pair has large magnitude off the coast, but the downscaling operator slight damps the pattern along the coast especially at the coast. The first and second singular pairs for the east coast are similar to that of the west coast, with the first one being a coherent structure and the second one being a dipole-like structure (Fig. S5). Note that the changing sign of the anomalies when moving from the coast to the offshore region indicates the influence of the strength of the boundary current on the coastal sea level variability through geostrophic balance.

In addition, to assess the importance of each singular vector pair in the downscaling, we reconstructed the downscaling operator **B** using different SV truncations. Then the different downscaling operator **B** was used to downscale the hindcast and the skill of the downscaled hindcast are accessed.

The skills of the downscaled hindcast using different truncation of the singular vectors (SVs) in Fig. S4-5 are shown in Fig. S6. For the west coast, the first SV pair is the most important while the skill is gradually improved by adding more SV pairs in the downscaling operator, with the exception for San Francisco. For the Virginia Key and Charleston, only the first pair of the SVs matters for the skill, and the skill degrades if adding more SVs in the downscaling operator. For Atlantic City, adding more SVs slightly improves the skill, but it is presumably due to the trend component in the dataset (not shown).

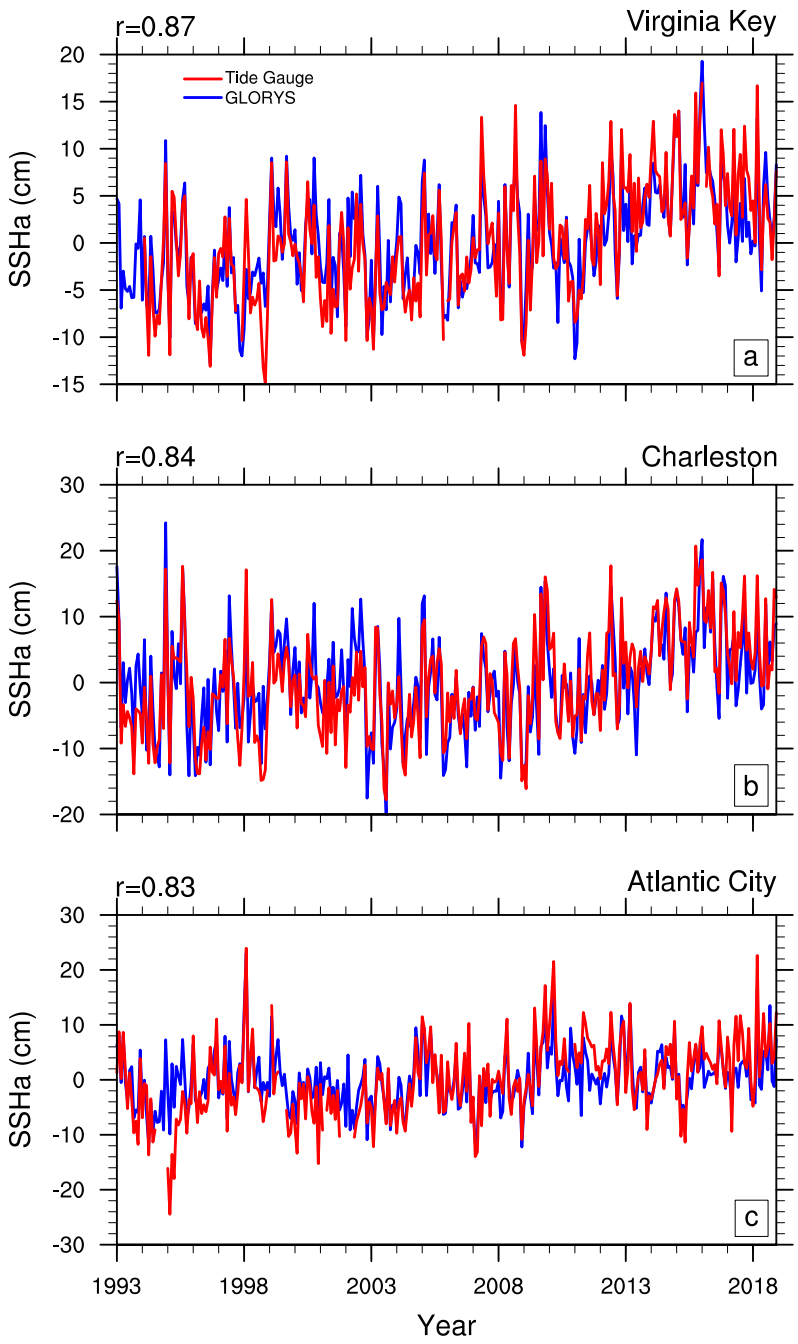

Fig. S1 The sea level anomalies for (a) Virginia Key, (b) Charleston and (c) Atlantic City, from GLORYS (blue) and tide gauge observation (red). The correlation coefficient between tide gauge observation and GLORYS for each station is shown on top of each panel. The nearest grid point in the GLORYS grids to each the tide gauge location is used. The unit is centimeter.

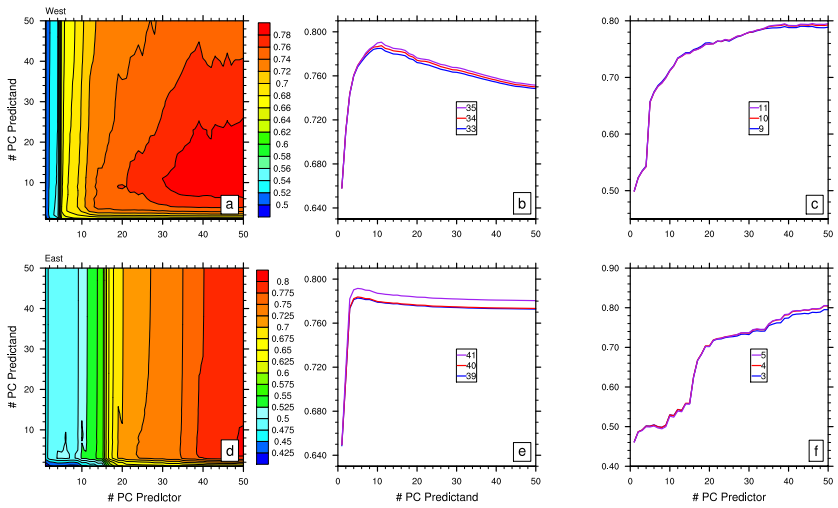

Figure S2. Space and time aggregated correlation coefficient between the SSH anomalies from GLORYS reanalysis and the observational downscaled SSH anomalies for (a,b,c) West Coast and (d,e,f) East Coast. (a,d) show the correlation coefficient as a function of the EOF truncation for predictor and predictand; and (b,c,e,f) show the correlation coefficient as a function of the EOF truncation for the predictor (predictand) with the predictand (predictor) fixed.

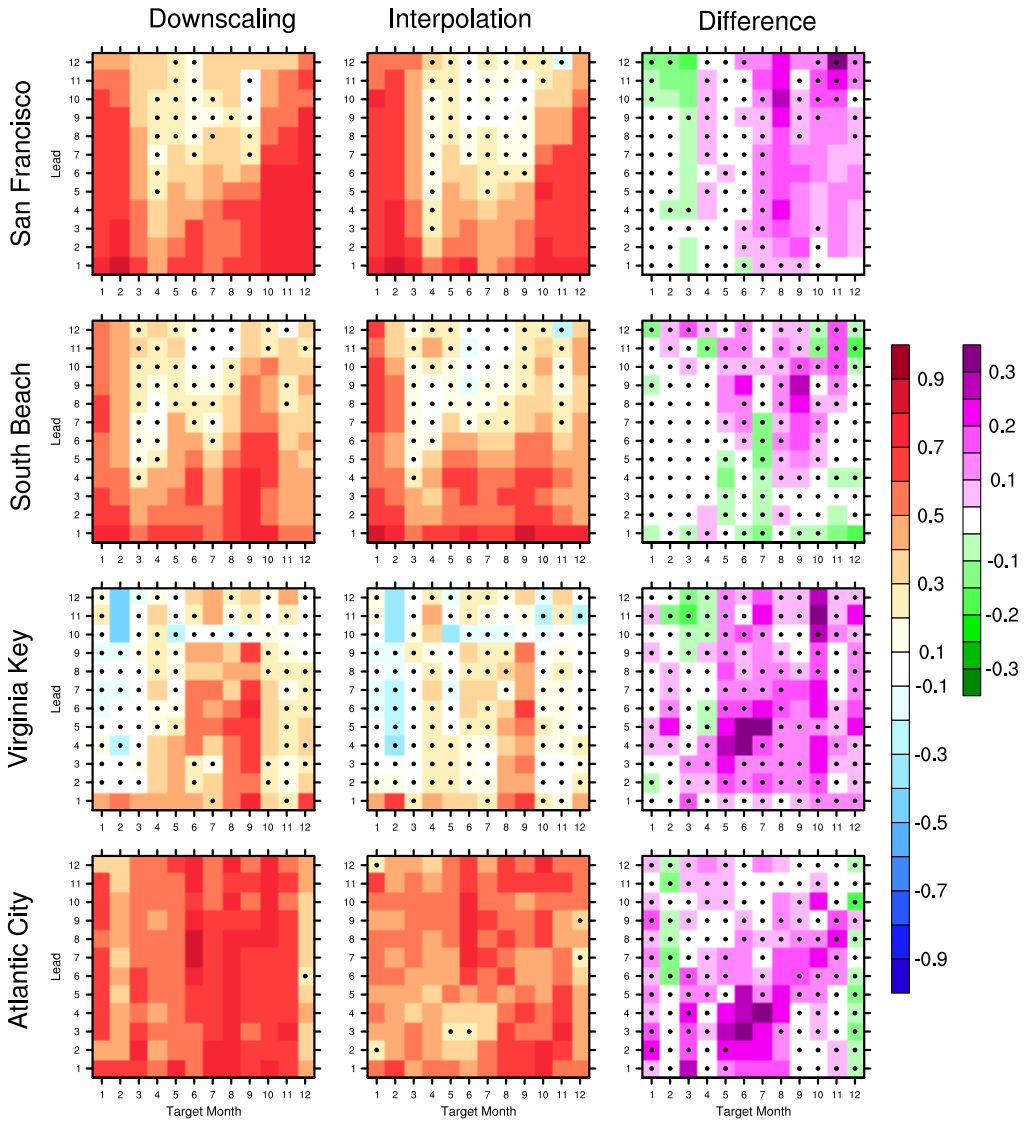

Figure S3. The Anomaly Correlation of the ensemble mean of downscaling (left column) and interpolation (middle column) of the hindcast, verified against the tide gauge observation at San Francisco, South Beach, Virginia Key and Atlantic City, for each lead time and target month; the right column shows the AC difference of downscaling and interpolation of the hindcast (downscaling minus interpolation). The black dot indicates the correlation or correlation difference is not statistically significant at 0.1 level at that lead time and target month.

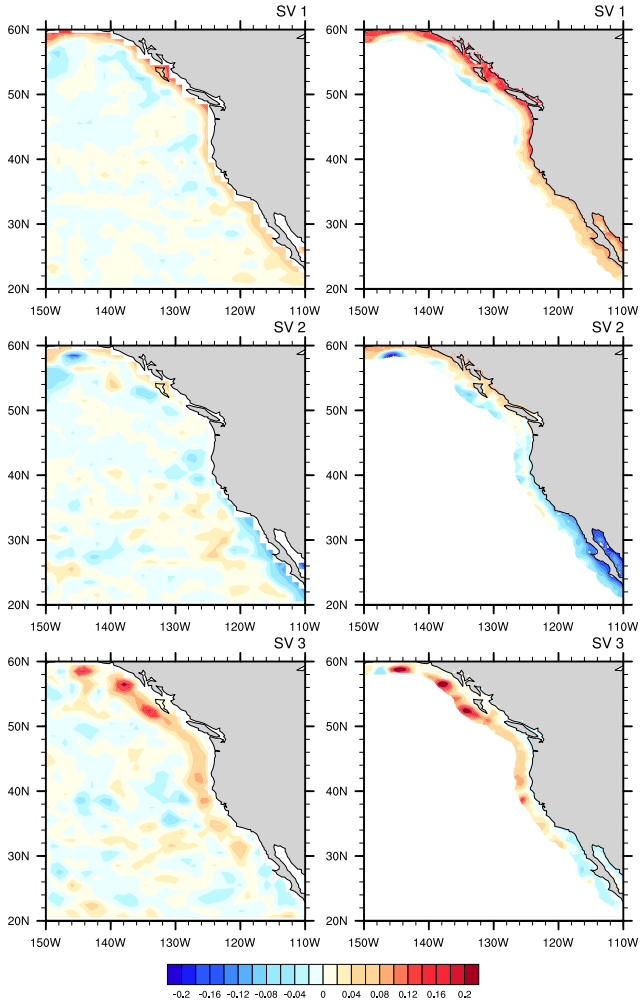

Fig. S4 The first three singular vector pairs from SVD of the regression matrix of the downscaling for the West Coast. Left column corresponds to the singular vectors related to predictor, and right column corresponds to the singular vectors related to predictor. The right column was weighted by the corresponding singular values so that the relative magnitude change from left column to right column represents the amplification from the regression matrix. The regression matrix is in EOF space, and the singular vector are reconstructed using the respective EOF patterns from reanalysis. The units of the singular vectors are arbitrary.

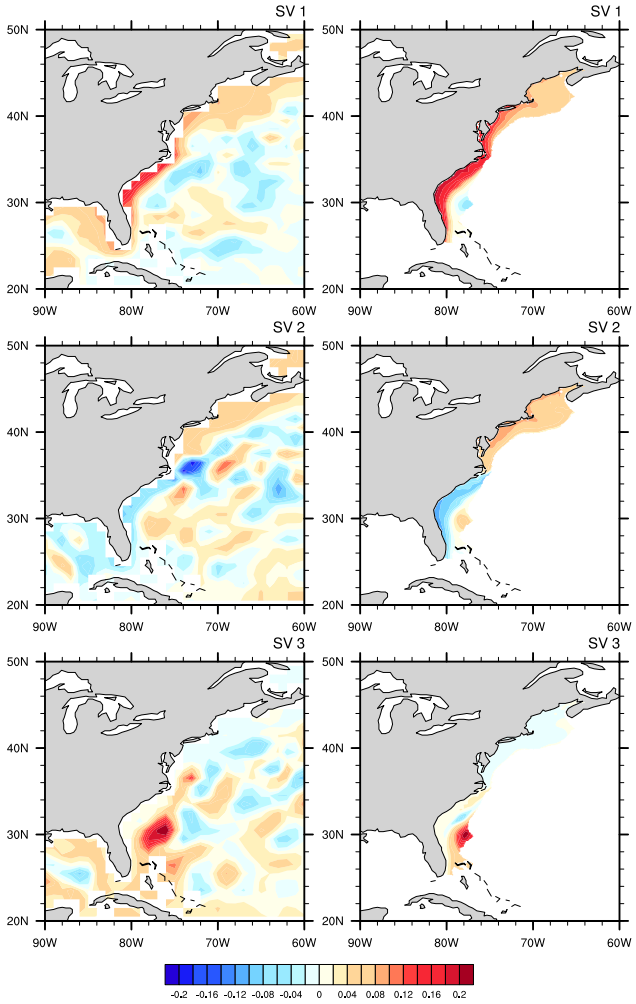

Fig. S5 Same as Figure S5 but for the East Coast.

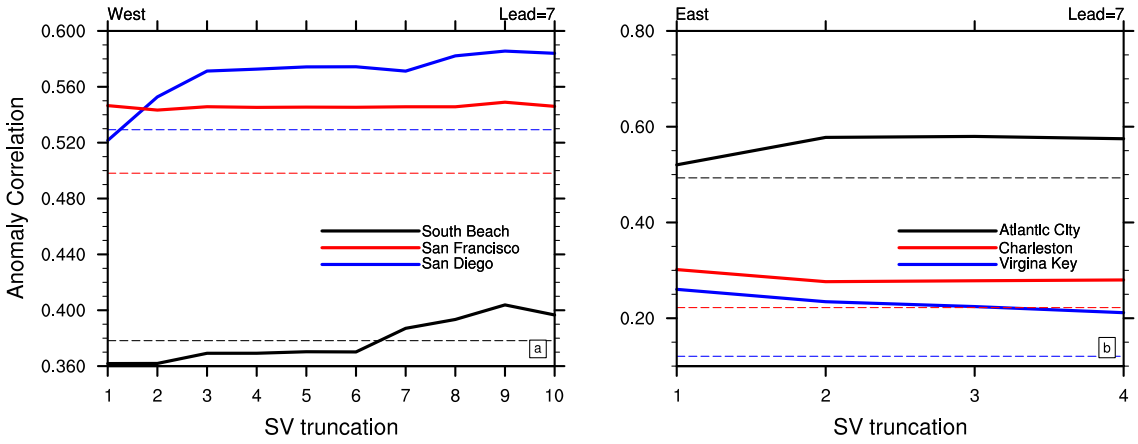

Fig. S6 The anomaly correlation between the downscaled hindcast (solid lines) or interpolated hindcast (dash lines) and the tide gauge observation for three tide gauge stations at (a) west coast and (b) east coast. The downscaled hindcast is constructed using different truncation of the singular vectors in the SVD of the regression matrix (see details in Text S1).

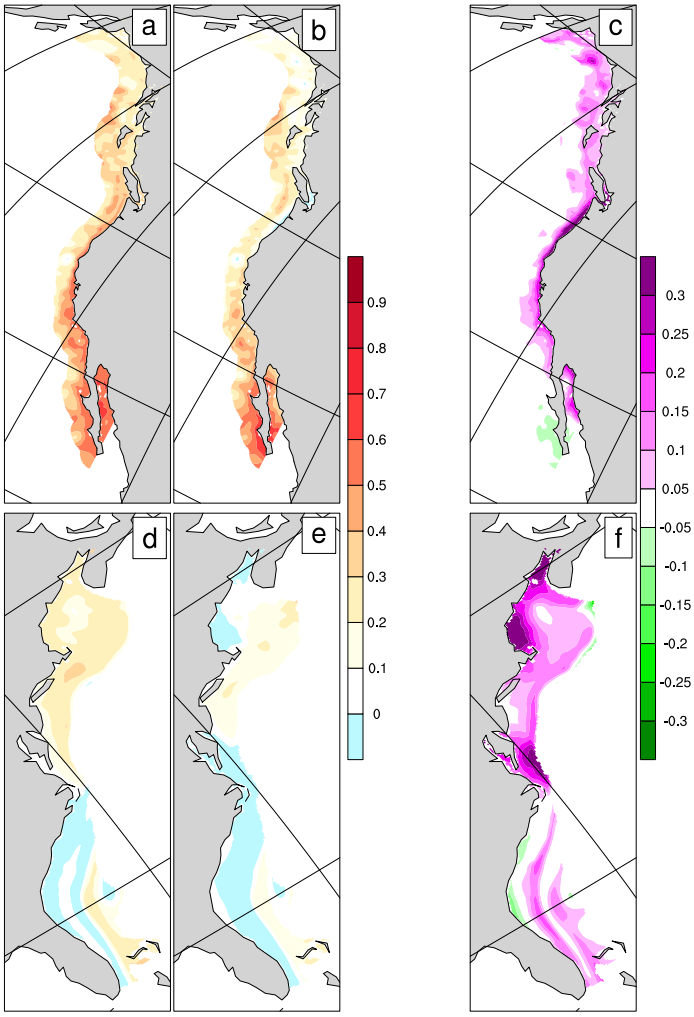

Fig. S7 Anomaly correlation for Lead-7 month of (a,d) the downscaled hindcast and (b,e) the interpolated hindcast from CanCM3, verified against SSH anomaly from GLORYS reanalysis; (c,f) are the correlation difference between downscaling and interpolation.

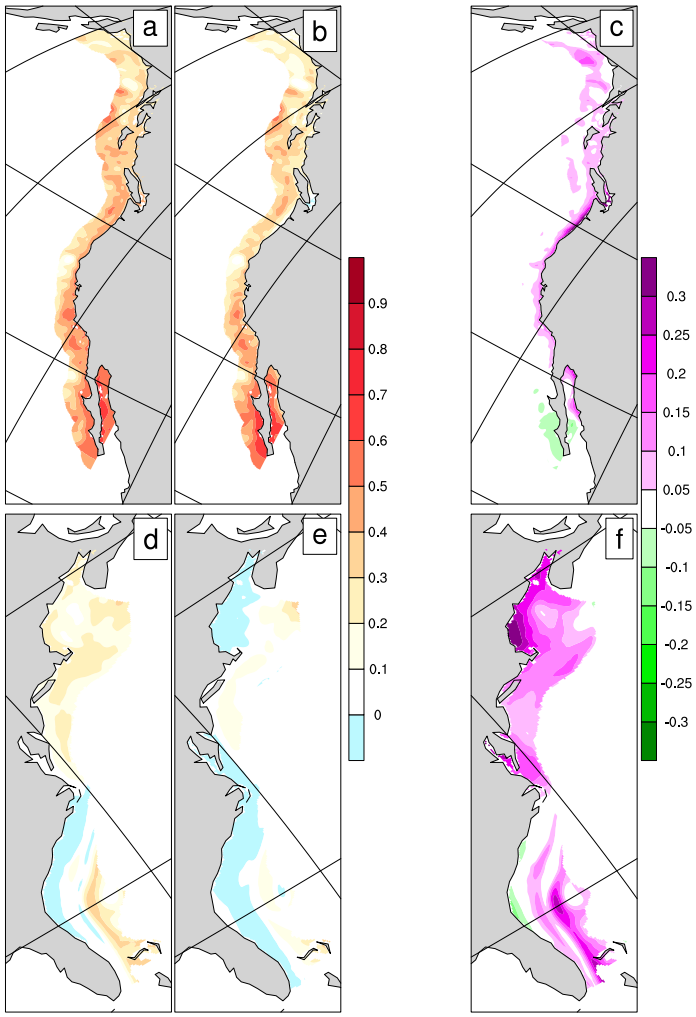

Fig. S8 Same as Fig S7 but for CanCM4 model.

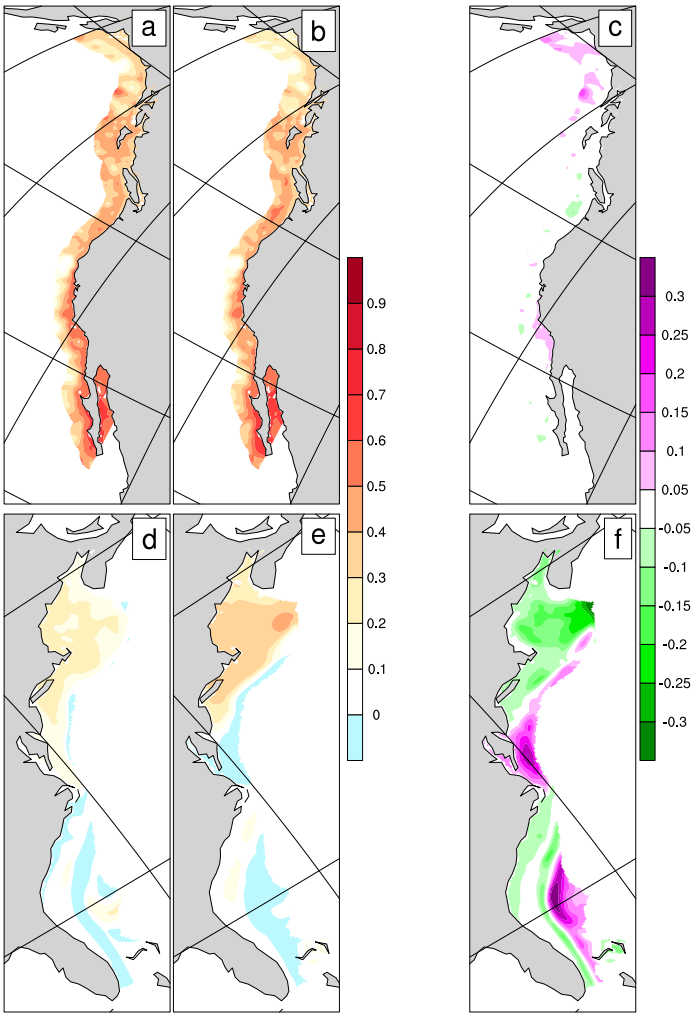

Fig. S9 Same as Fig. S7 but for CCSM4-UM model.

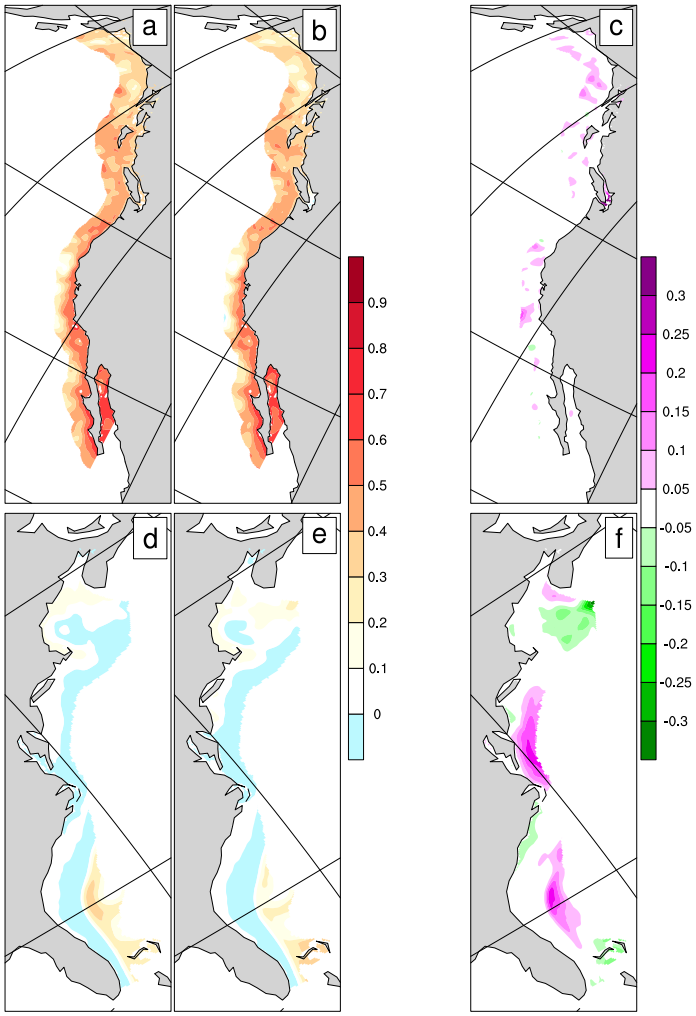

Fig. S10 Same as Fig. S7 but for CFSv2 model.

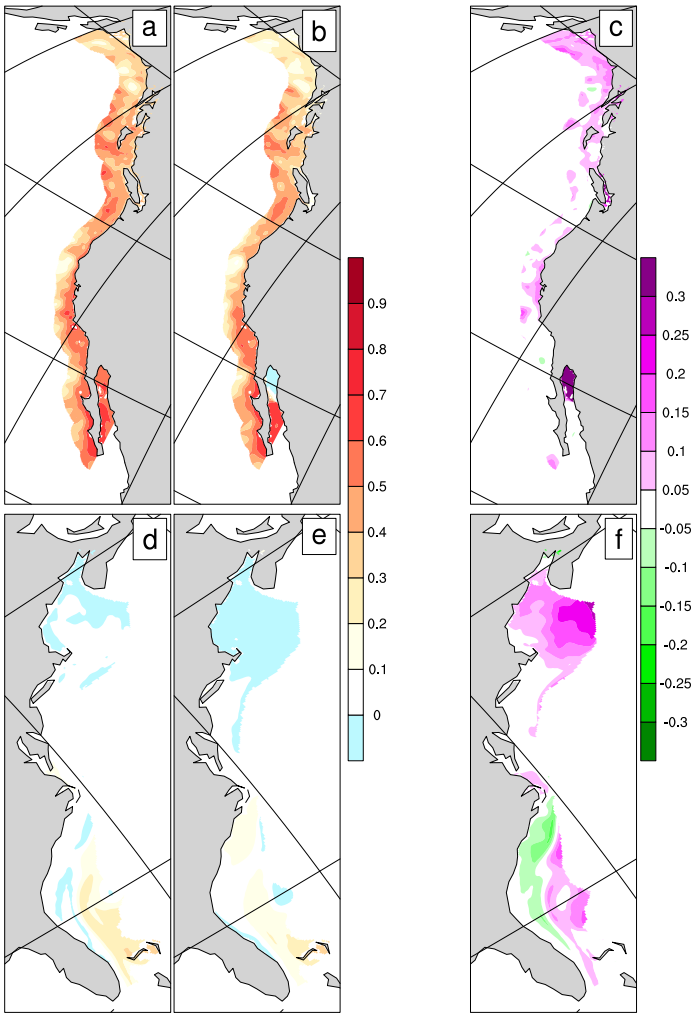

Fig. S11 Same as Fig. S7 but for GFDL model.

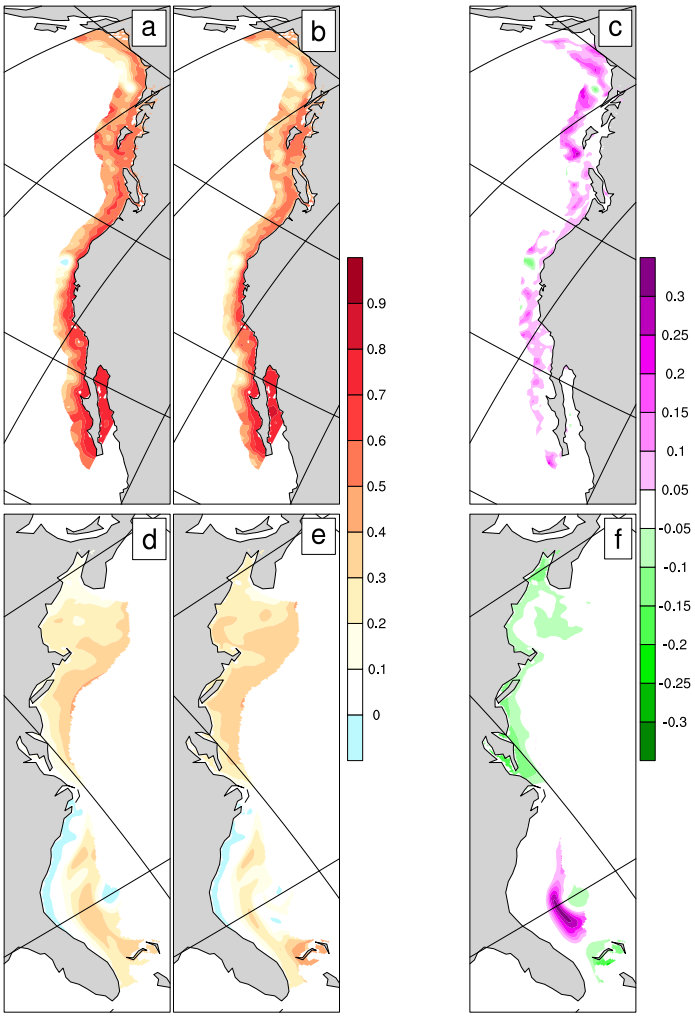

Fig. S12 Same as Fig. S7 but for ACCESS-S2 model.

Model	Organization	Ensemble size	Lead times	Resolution	Reference
(1) ACCESS-S2	Australian Bureau of Meteorology	12	1-9	0.25°	
(2) CanCM3	Canadian Meteorological Centre	10	1-12	1°	Merryfield et al. (2013)
(3) CanCM4	Canadian Meteorological Centre	10	1-12	1°	Merryfield et al. (2013)
(4) CCSM4-UM	University of Miami	10	1-12	1°	Kirtman et al. (2014)
(5) CFSv2	National Centers for Environmental Prediction	24 (28)	1-10	0.5°	Saha et al. (2014)
(6) GFDL CM2.1	Geophysical Fluid Dynamics Laboratory	10	1-12	1°	Zhang et al. (2007)

Table S1. Description of the 6 retrospective forecast systems used in this study. For each model system, the corresponding organization, ensemble size, maximum lead (months), nominal horizontal resolution of the ocean component (degrees), and a reference are indicated.